First-order phase transition of fixed connectivity surfaces

Hiroshi Koibuchi,* Nobuyuki Kusano, Atsusi Nidaira, and Komei Suzuki
Department of Mechanical Engineering, Ibaraki College of Technology, Nakane 866 Hitachnaka, Ibaraki 312-8508, Japan

Mitsuru Yamada
Department of Mathematical Sciences, Faculty of Sciences, Ibaraki University, Bunkyo 2-1-1, Mito, Ibaraki 310-8512, Japan
(Received 7 January 2004; published 23 June 2004)

We report numerical evidence of the discontinuous transition of a tethered membrane model which is defined within a framework of the membrane elasticity of Helfrich. Two kinds of phantom tethered membrane models are studied via the canonical Monte Carlo simulation on triangulated fixed connectivity surfaces of spherical topology. One surface model is defined by the Gaussian term and the bending energy term, and the other, which is tensionless, is defined by the bending energy term and a hard wall potential. The bending energy is defined by using the normal vector at each vertex. Both models undergo the first-order phase transition characterized by a gap of the bending energy. The phase structure of the models depends on the choice of discrete bending energy.

I. INTRODUCTION

Tethered membrane models [1–4] are ordinarily defined by a Hamiltonian that is a linear combination of discrete bending energy and surface tension energy [5,6]. Hence, there may be a variety of statistical models of membranes, since discrete Hamiltonians can be chosen arbitrarily even within the Helfrich or Polyakov-Kleinert prescription of membranes. As a consequence, it is natural to ask whether the phase structure [7–11] of the model depends on the Hamiltonian.

However, little attention has been given to the dependence of the phase transition on the Hamiltonian of tethered surfaces both for models that have surface tension [12–21] and for tensionless models [22–27]. Almost all numerical studies done so far utilize the bending energy of the ordinary form $1 - \mathbf{n}_i \cdot \mathbf{n}_j$, where $\mathbf{n}_i$ is the normal vector of triangle i.

One other discrete bending energy that has been utilized by Gompper and Kroll [28] is based on the discretization of the Laplacian in the dual lattice formulation of discrete mechanics by Lee [29]. Similar discrete bending energy was adopted in Refs. [14,17,30]. Both discrete bending energies give results compatible with the continuous phase transition of the model [7–11].

Recently, it was reported [31] that a tethered membrane model with ordinary bending energy undergoes the discontinuous phase transition predicted in [32], although the Lennard-Jones (LJ) potential is assumed to serve as the Gaussian term. Hence, we thinkit is worthwhile to show that the discontinuous phase transition can be seen in a tethered membrane model when the Hamiltonian is defined only by a discretization of the Helfrich Hamiltonian.

The purpose of this paper is to show numerical evidence that the phase structure of phantom tethered models depends on the choice of the discrete bending energy. By using the normal vector at each vertex, we define a bending energy which is different from the ordinary one. We will study two kinds of models: one is a model that has the Gaussian term for surface tension and the other is a tensionless model that has no surface tension term but has a hard wall potential. It will be shown that both models undergo a first-order phase transition.

II. MODEL AND MONTE CARLO TECHNIQUES

Membrane models are ordinarily defined by the discrete Hamiltonian $S = S_1 + b S_2$ with bending rigidity b, where S_1 is the surface tension energy and S_2 is the bending energy, respectively, defined by

$$S_1 = \sum_{(ij)} (X_i - X_j)^2, \quad S_2 = \sum_{(ij)} (1 - \mathbf{n}_i \cdot \mathbf{n}_j). \quad (1)$$

$\Sigma_{(ij)}$ in Eq. (1) is over all bonds (ij), and $\mathbf{n}_i$, $\mathbf{n}_j$ are the unit normal vectors of the triangles sharing the bond (ij). X_i ($\in \mathbb{R}^3$) in S_1 is the position of the vertex i.

The other possible bending energy S_2 can be obtained by using the normal vector of the vertex i such as

$$\mathbf{n}(i) = \frac{\mathbf{N}_i}{|\mathbf{N}_i|}, \quad \mathbf{N}_i = \sum_{j(i)} \mathbf{n}_{j(i)} A_{\Delta_{j(i)}}, \quad (2)$$

where $\Sigma_{j(i)}$ denotes the summation over triangles $j(i)$ linked to the vertex i. The vector $\mathbf{n}_{j(i)}$ is the unit normal of the triangle $j(i)$, and $A_{\Delta_{j(i)}}$ is the area of $j(i)$.

The new discrete bending energy can be obtained by using the normal vector of Eq. (2). Thus, we have

$$S_2 = \sum_i \sum_{j(i)} [1 - \mathbf{n}(i) \cdot \mathbf{n}_{j(i)}], \quad (3)$$

which is clearly different from that of Eq. (1). It should be noted that $S_2(\text{illdef}) = \Sigma_{i,j}[1 - \mathbf{n}(i) \cdot \mathbf{n}(j)]$ defined only by using

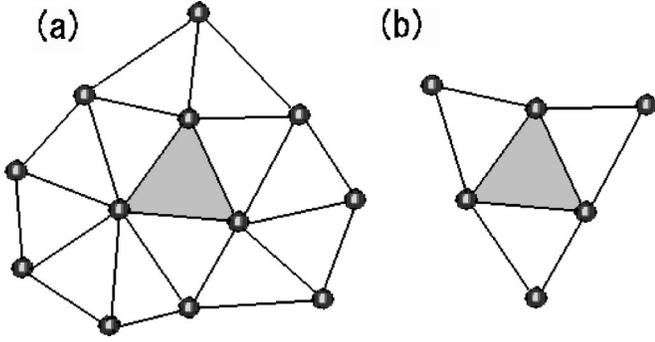*Electronic address: koibuchi@mech.ibaraki-ct.ac.jp

FIG. 1. (a) Ranges of interaction between normal vectors of triangles for S_2 in Eq. (3) and (b) those for S_2 in Eq. (1). The normal vector of the shaded triangle interacts with those of the surrounding triangles in (a) and (b). Small spheres represent vertices.

FIG. 2. (a) S_1/N_B vs b of model 1 and (b) S_1/N_B vs b of model 2, where N_B is the total number of bonds. $N=1500$.

the normal vectors $\mathbf{n}(i)$ in Eq. (2) is not well defined. This ill definedness comes from the fact that there exist two surfaces locally different from each other that have the same value of S_2(illdef). Two normal vectors at the ends of a bond (i,j) can be parallel for surfaces that are not smooth.

We study two kinds of models in this paper. The first, which will be denoted by model 1, is a model defined by

$$Z_1 = \int \prod_{i=1}^{N} dX_i \exp[-(S_1 + bS_2)], \quad \text{(model 1)},$$

$$S_1 = \sum_{(ij)} (X_i - X_j)^2, \quad S_2 = \sum_{i} \sum_{j(i)} [1 - \mathbf{n}(i) \cdot \mathbf{n}_{j(i)}], \quad (4)$$

where the center of the surface is fixed to remove the translational zero mode. S_2 is identical with Eq. (3).

The second model, which will be denoted by model 2, is a tensionless model defined by

$$Z_2 = \int \prod_{i=1}^{N} dX_i \exp[-(bS_2 + V)], \quad \text{(model 2)},$$

$$S_2 = \sum_{i} \sum_{j(i)} [1 - \mathbf{n}(i) \cdot \mathbf{n}_{j(i)}], \quad (5)$$

where S_2 is identical with that of model 1 in Eq. (4) and V is the hard wall potential defined by

$$V(|X_i - X_j|) = \begin{cases} 0 & (0 < |X_i - X_j| < r_0), \\ \infty & \text{(otherwise)}. \end{cases} \quad (6)$$

The value of r_0 on the right-hand side of Eq. (6) is fixed to $r_0 = \sqrt{1.15}$. As a consequence we have $\langle \Sigma(X_i - X_j)^2 \rangle/N \simeq 3/2$, which holds for model 1 which contains the Gaussian term S_1. It should be noted that model 2 is considered to be independent of the hidden length introduced by r_0. The Monte Carlo (MC) results are independent of the value of r_0. This was, in fact, precisely checked in Ref. [15].

Figures 1(a) and 1(b) show the range of interactions described by S_2 in Eq. (3) and the ordinary S_2 in Eq. (1). A difference between S_2 in (3) and S_2 in Eq. (1) can be seen in the number of triangles whose normal vectors interact with
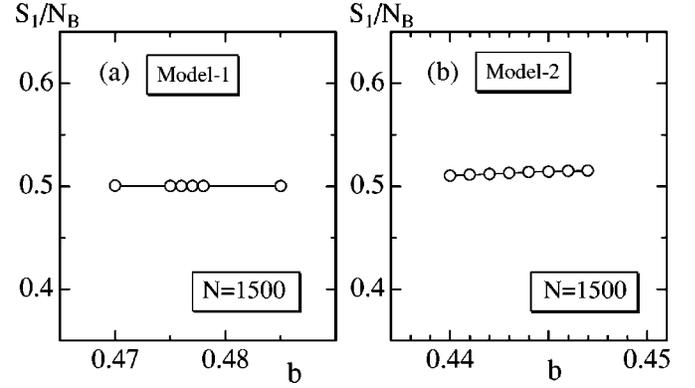
the one of a given triangle, which is shaded in Figs. 1(a) and 1(b). The number of triangles for S_2 in Eq. (3) is dependent on a given triangle and hence locally changes, while the number for S_2 in Eq. (1) is always 3.

We use the canonical Metropolis Monte Carlo technique. Spheres are triangulated by linking uniformly scattered points. The histograms of coordination number of surfaces are identical with those shown in Ref. [15].

The position X of vertices is updated with the MC technique by moving the current position X to a new position $X'=X+\delta X$, where δX is chosen in a small sphere by using uniform random numbers. The radius R_0 of the small sphere is fixed to $R_0=\epsilon l_0$, where l_0 is the mean bond length which is computed at every 250 MCS (Monte Carlo sweeps), and a constant ϵ is fixed at the beginning of the simulation to maintain 50% –55% acceptance rate for model 1 and 55% –65% for model 2. The radius R_0 becomes almost constant, because l_0 is constant in the equilibrium configurations.

We impose the lower bound $10^{-6}A_0$ on the area of triangles, where A_0 is the mean area of triangles computed at every 250 MCS. As a consequence, updates of X are constrained so that the resulting area of the triangles becomes larger than $10^{-6}A_0$. However, the areas of almost all triangles are larger than $10^{-6}A_0$ in our MC simulations without the lower bound; hence, it seems that the areas are almost free from such a constraint. No constraint is imposed on the bond length.

III. RESULTS

We first show S_1/N_B of model 1 and model 2, respectively, in Figs. 2(a) and 2(b), where N_B is the total number of bonds. It should be noted that S_1/N_B is the mean bond length squared l_0^2. S_1/N_B in Fig. 2(a) of model 1 is completely compatible with the expected result $S_1/N=3/2$, since $N_B=3N-6(\simeq 3N)$ on the spherical surfaces. In fact, a typical sample in Fig. 2(a) is $S_1/N_B=0.500\,15\pm0.000\,12$ at $b=0.476$. Moreover, S_1/N_B in Fig. 2(b) of model 2 is also compatible with our expectation $S_1/N\simeq 3/2$ as already stated in the paragraph below Eq. (6), although the Gaussian term S_1 is not included in the Hamiltonian of model 2. Thus, we confirmed that l_0 is constant in the equilibrium configurations in both models.
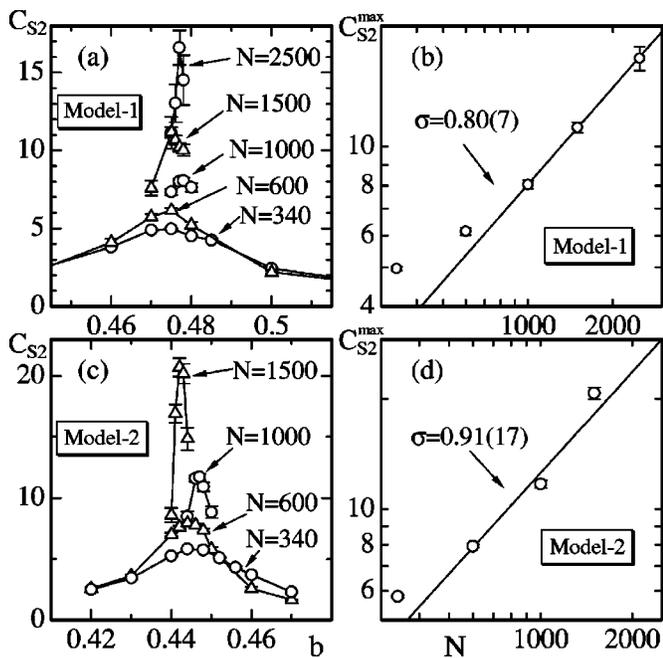
FIG. 3. (a) C_{S_2} vs b and (b) $C_{S_2}^{max}$ vs N in log-log scale. Both (a) and (b) are obtained by model 1 whose Hamiltonian is S_1+bS_2. (c) C_{S_2} vs b and (d) $C_{S_2}^{max}$ vs N in log-log scale. Both (c) and (d) are obtained by model 2 whose Hamiltonian is bS_2+V.

FIG. 4. (a) Variation of S_2/N_B against the number of MCS and (b) the histogram $h(S_2/N_B)$, obtained by model 1. The results obtained by model 2 are shown in (c) and (d).

The specific heat C_{S_2} is a fluctuation of the bending energy and is given by

$$C_{S_2} = \frac{b^2}{N}(\langle S_2^2\rangle - \langle S_2\rangle^2). \qquad (7)$$

Total number of MCS is about $0.8\sim1.0\times10^8$ for $N=340, N=600$, 1.5×10^8 for $N=1000$, 3×10^8 for $N=1500$, and 2.2×10^8 for $N=2500$ at the transition points $b_c(N)$ for model 1. The number of MCS at $b\neq b_c(N)$ is relatively small. The total number of MCS for model 2 is smaller than that for model 1, since the speed of convergence of model 2 is relatively faster than model 1.

Figure 3(a) shows C_{S_2} vs b of model 1. The peak values $C_{S_2}^{max}$ of model 1 are plotted in Fig. 3(b) against N in a log-log scale. Figures 3(c) and 3(d) are results obtained by model 2. The number of molecules is $N=340$, $N=600$, $N=1000$, and $N=1500$ for model 2.

The slope of the straight lines in Figs. 3(b) and 3(d) represents the critical exponent σ defined by

$$C_{S_2}^{max} \sim N^{\sigma}. \qquad (8)$$

The largest three data in each figure are included in the fit, and we have

$$\sigma_1 = 0.798(66) \quad \text{(model 1)},$$

$$\sigma_2 = 0.914(166) \quad \text{(model 2)}.$$

The value $\sigma_1=0.798(66)$ is smaller than 1 and hence implies that the order of the phase transition of model 1 is of second order. However, as we will see next, the order of the phase
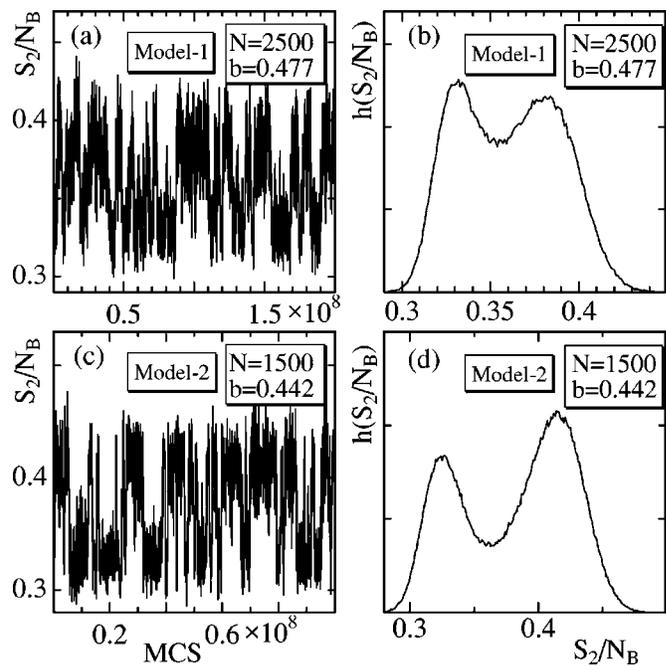
transition of model 1 is considered to be of first order. While $\sigma_1<1$, the value $\sigma_2=0.914(166)$ almost equals to 1 and hence suggests that model 2 undergoes a first-order phase transition.

To clarify the order of the transition of model 1, we plot in Fig. 4(a) the variation of S_2/N_B against the number of MCS. The series S_2 shown in Fig. 4(a) was obtained at every 5×10^4 MCS at the transition point $b=b_c(N)$ on the surface of size $N=2500$. The corresponding histogram $h(S_2/N_B)$ is drawn in Fig. 4(b). Figures 4(c) and 4(d) are the results obtained by model 2 of size $N=1500$.

We clearly see in Fig. 4(a) that there are two distinct states which represent a discontinuous phase transition in model 1. The histogram in Fig. 4(b) shows more clearly the existence of the two states separated by a gap of S_2 in model 1. It is also easy to understand from Figs. 4(c) and 4(d) that model 2 undergoes a first-order phase transition characterized by a gap of S_2.

The mean-square size X^2, defined by

$$X^2 = \frac{1}{N}\sum_i (X_i - \bar{X})^2, \quad \bar{X} = \frac{1}{N}\sum_i X_i, \qquad (9)$$

is plotted in Fig. 5(a) against the number of MCS of model 1. The corresponding histogram $h(X^2)$ is drawn in Fig. 5(b). Figures 5(c) and 5(d) are the results obtained by model 2. We see two different sizes at the transition point in each model and hence consider that the phase transitions in both models are characterized also by the discontinuity of X^2. The reason why we use X^2 obtained at $b=0.443$ in Figs. 5(c) and 5(d) is that the double peaks in the histogram of X^2 at $b=0.443$ are
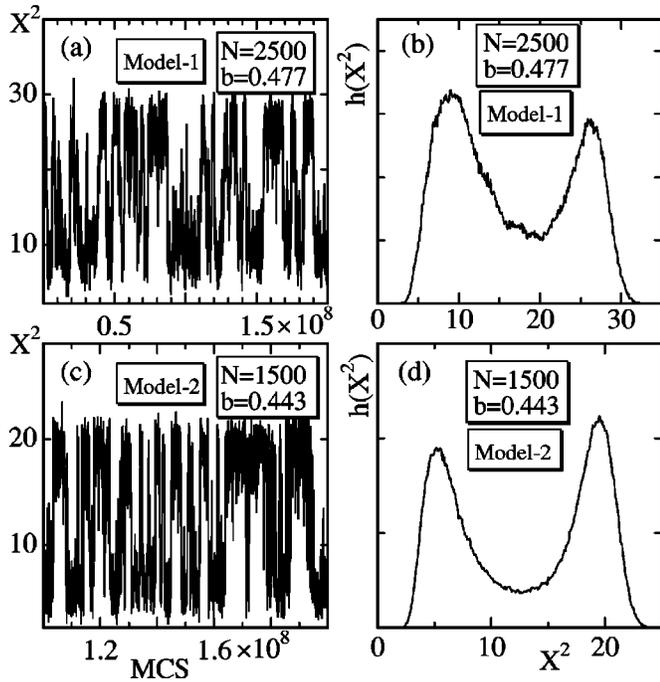
FIG. 5. (a) Variation of X^2 against the number of MCS and (b) the histogram $h(X^2)$, obtained by model 1. The results obtained by model 2 are shown in (c) and (d).

FIG. 6. (a) X^2 vs b of model 1 and (b) X^2 vs N at the transition point $b=b_c(N)$. The results obtained by model 2 are shown in (c) and (d).

clearer than at $b=0.442$ where the histogram of S_2/N_B plotted in Figs. 4(c) and 4(d) were obtained.

The Hausdorff dimension [33–35] is defined by

$$X^2 \sim N^{2/H}. \qquad (10)$$

The gap of X^2 at the transition point implies that H discontinuously changes at that point.

We plot in Fig. 6(a) X^2 vs b of model 1. The mean square size X^2 at $b=b_c(N)$ is plotted against N in a log-log scale in Fig. 6(b). The straight line denoted by *smooth* is obtained by fitting X^2, each of which isthe larger X^2 in the double peaks shown in Fig. 5(b). Another straight line denoted by *crumpled* is obtained by fitting the smaller X^2 in the peaks. Errors of X^2 were not included in the least-squares fitting, since the fitting was done by using only the peak values of X^2 in the histogram shown in Fig. 5(b). Figures 6(c) and 6(d) show the results of model 2.

From the slope of the straight lines in Figs. 6(b) and 6(d), we have

$$H_1(\uparrow) = 2.13(17), \quad H_1(\downarrow) = 3.66(107) \quad \text{(model 1)},$$

$$H_2(\uparrow) = 2.16(30), \quad H_2(\downarrow) = 7.84(977) \quad \text{(model 2)}. \qquad (11)$$

$H(\uparrow)[H(\downarrow)]$ is considered as the Hausdorff dimension in the smooth [crumpled] phase at $b>b_c$ [$b<b_c$] just above [below] b_c in each model. The reason for the large errors in both
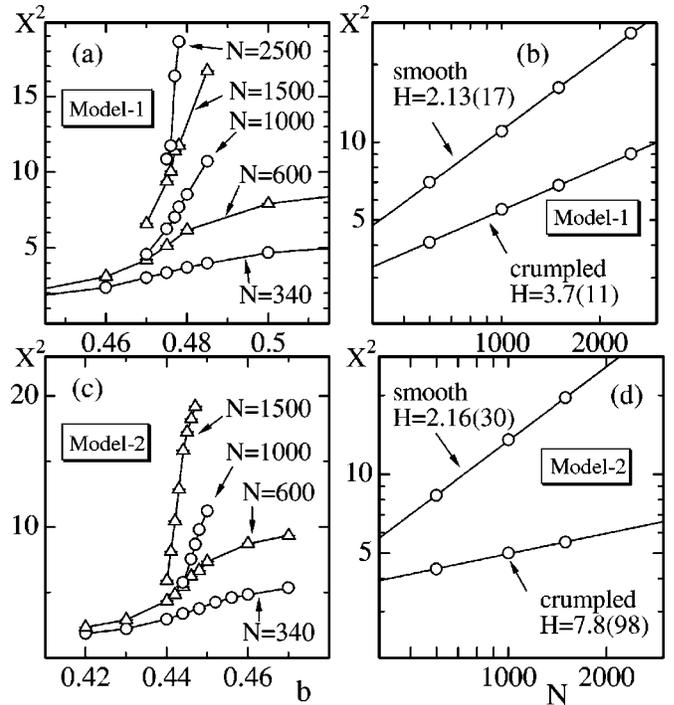
$H_1(\downarrow)$ and $H_2(\downarrow)$ seems come from the fact that there are a few data points of X^2 included in the fitting.

We understand from the straight lines in Figs. 6(b) and 6(d) that the phase transition of model 2 is relatively stronger than that of model 1, although both transition are of first order. The gap of H at $b=b_c$ of model 2 is relatively larger
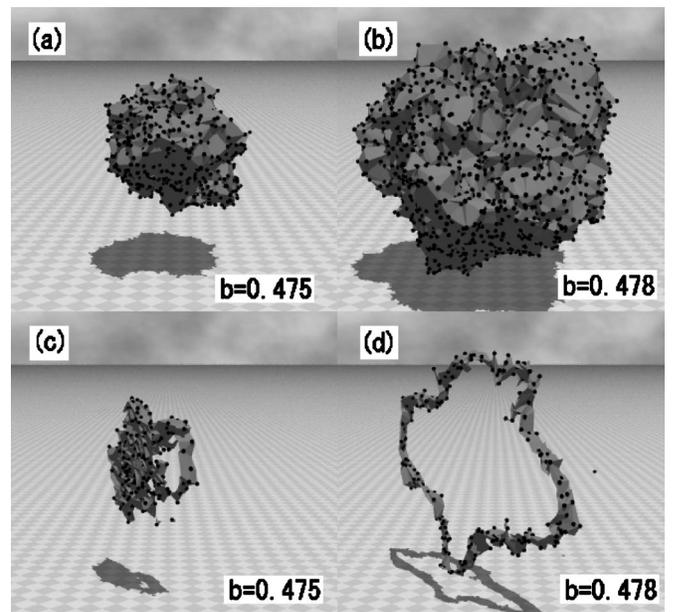

FIG. 7. Snapshots of model 1 surfaces obtained at (a) b =0.475 (crumpled phase), (b) $b=0.478$ (smooth phase), and the sections of the surfaces in (a) and (b) are shown in (c) and (d), respectively. $N=2500$.

than that of model 1; this difference of H can be visible in the slope of the straight lines in Figs. 6(b) and 6(d).

There is no difference between the surfaces in the smooth phase of the models in this paper and those of [15], while the surfaces in the disordered (or crumpled) phase of the models in this paper are more crumpled than those in [15]. The Hausdorff dimension at $b > b_c$ of the models and those of [15] are comparable, although the order of the transition of the models in this paper is different from that in [15]; the models in [15] have a continuous phase transition.

We note also that both $H_1(\uparrow)$ and $H_2(\uparrow)$ are compatible with (or slightly smaller than) the Flory prediction $H = 2.5$, and they are almost compatible with an analytical result $H = 2.39(23)$ which corresponds to the scaling exponent $\nu = 0.84 \pm 0.04$ in [36] where $\nu = 2/H$. The values $H_1(\uparrow)$ and $H_2(\uparrow)$ in Eq. (11) imply that the surfaces are relatively swollen and smooth in the smooth phase at $b > b_c$ in both models.

In order to see the surfaces, we show snapshots of size $N = 2500$ of model 1 in Figs. 7(a) and 7(b), one of which is obtained in the crumpled phase at $b = 0.475$ and the other in the smooth phase at $b = 0.478$. The sections of them are shown in Figs. 7(c) and 7(d). The surface swells in the smooth phase as expected. We also find that the surface in Fig. 7(b) is smooth only at long-range scales and rough at short scales. This is compatible with that seen inthe model with ordinary bending energy [15]. The surfaces of model 2 are almost the same as those in Fig. 7.

IV. SUMMARY AND CONCLUSIONS

We have shown that the continuous phase transition seen in ordinary tethered membrane models is strengthened in two kinds of tethered membrane models, whose bending energy is defined by using the normal vectors at the vertices. One of the models is defined by the Hamiltonian $S_1 + bS_2$, and the other is a tensionless model defined by $bS_2 + V$, where V is a hard wall potential. It was shown by extensive MC simulations that both of the models undergo a first-order phase transition which is characterized by a gap of S_2. The size of the spherical surfaces and the Hausdorff dimension discontinuously change at the phase transition in both models.

The definition of the Hamiltonian remains in the framework of the membrane elasticity of Helfrich. The bending energy in Eq. (3) utilized in this paper appears to induce a non-nearest-neighbor interaction between normal vectors of the surface. In fact, the range of the interaction is a bit larger than that of the ordinary bending energy as depicted in Fig. 1. However, the bending energy in Eq. (3) is written by the normal vectors of Eq. (2) and the normal vectors of the neighboring triangles, and hence it is defined only by local geometric quantities of the surface just like the ordinary bending energy in Eq. (1).

ACKNOWLEDGMENT

[1] F. David, in *Two Dimensional Quantum Gravity and Random Surfaces*, edited by D. Nelson, T. Piran, and S. Weinberg (World Scientific, Singapore, 1989), Vol. 8, p. 81.
[2] J. F. Wheater, J. Phys. A **27**, 3323 (1994).
[3] K. Wiese, in *Phase Transitions and Critical Phenomena*, edited by C. Domb and J. Lebowitz (Academic Press, London, 2000), Vol. 19, p. 253.
[4] M. Bowick and A. Travesset, Phys. Rep. **344**, 255 (2001).
[5] W. Helfrich, Z. Naturforsch. C **28**, 693 (1973).
[6] A. M. Polyakov, Nucl. Phys. B **268**, 406 (1986); H. Kleinert, Phys. Lett. B **174**, 335 (1986).
[7] L. Peliti and S. Leibler, Phys. Rev. Lett. **54**, 1690 (1985).
[8] F. David and E. Guitter, Europhys. Lett. **5**, 709 (1988).
[9] F. David, Europhys. Lett. **2**, 577 (1986).
[10] M. E.S. Borelli, H. Kleinert, and Adriaan M.J. Schakel, Phys. Lett. A **267**, 201 (2000).
[11] M. E.S. Borelli and H. Kleinert, Europhys. Lett. **53**, 551 (2001).
[12] J. F. Wheater, Nucl. Phys. B **458**, 671 (1996).
[13] M. Bowick, S. Catterall, M. Falcioni, G. Thorleifsson, and K. Anagnostopoulos, J. Phys. I **6**, 1321 (1996); Nucl. Phys. B (Proc. Suppl.) **47**, 838 (1996); **53**, 746 (1997).
[14] H. Koibuchi and M. Yamada, Int. J. Mod. Phys. C **11**, 1509 (2000).
[15] H. Koibuchi, N. Kusano, A. Nidaira, K. Suzuki, and T. Suzuki, Phys. Lett. A **314**, 1 (2003).
[16] S. M. Catterall, J. B. Kogut, and R. L. Renken, Nucl. Phys. B (Proc. Suppl.) **99A**, 1 (1991).
[17] H. Koibuchi and M. Yamada, Int. J. Mod. Phys. C **11**, 441 (2000).
[18] H. Koibuchi, Phys. Lett. A **300**, 586 (2002); H. Koibuchi, N. Kusano, A. Nidaira, K. Suzuki, and M. Yamada, *ibid.* **319**, 44 (2003).
[19] J. Ambjorn, A. Irback, J. Jurkiewicz, and B. Petersson, Nucl. Phys. B **393**, 571 (1993).
[20] K. Anagnostopoulos, M. Bowick, P. Gottington, M. Falcioni, L. Han, G. Harris, and E. Marinari, Phys. Lett. B **317**, 102 (1993).
[21] M. Bowick, P. Coddington, L. Han, G. Harris, and E. Marinari, Nucl. Phys. B (Proc. Suppl.) **30**, 795 (1993); Nucl. Phys. B **394**, 791 (1993).
[22] Y. Kantor and D. R. Nelson, Phys. Rev. A **36**, 4020 (1987).
[23] Y. Kantor, in *Statistical Mechanics of Membranes and Surfaces*, edited by D. Nelson, T. Piran, and S. Weinberg (World Scientific, Singapore 1989), Vol. 5, p. 115.
[24] Y. Kantor, M. Kardar, and D. R. Nelson, Phys. Rev. A **35**, 3056 (1987).
[25] J. S. Ho and Baumgartner, Europhys. Lett. **12**, 295 (1990).
[26] G. Gompper and D. M. Kroll, Phys. Rev. E **51**, 514 (1995).
[27] M. J. Bowick, A. Cacciuto, G. Thorleifsson, and A. Travesset, Eur. Phys. J. E **5**, 149 (2001).
[28] G. Gompper and D. M. Kroll, J. Phys. I **I 6**, 1305 (1996).
[29] T. D. Lee, in *How Far Are We from the Gauge Forces*, Subnuclear Series, Vol. 21, edited by A. Zichichi (Kluwer Aca-

demic, Dordrecht, 1986), p. 15.

[30] H. Koibuchi and M. Yamada, Mod. Phys. Lett. A **4**, 2417 (1989).

[31] J-P. Kownacki and H. T. Diep, Phys. Rev. E **66**, 066105 (2002).

[32] M. Paczuski, M. Kardar, and D. R. Nelson, Phys. Rev. Lett. **60**, 2638 (1988).

[33] D. J. Gross, Phys. Lett. **138B**, 185 (1984).

[34] B. Duplantier, Phys. Lett. **141B**, 239 (1984).

[35] J. Jurkiewicz and A. Krzywicki, Phys. Lett. **148B**, 148 (1984).

[36] F. David and K. J. Wiese, Phys. Rev. Lett. **76**, 4564 (1996).